

Growth of C-Axis Textured AlN Films on Vertical Sidewalls of Si Micro-Fins

Mehrdad Ramezani¹, Valeriy Felmetzger², Nicholas Rudawski³, and Roozbeh Tabrizian^{1, a)}

¹*Electrical and Computer Engineering Department, University of Florida, Gainesville, Florida 32611, USA*

²*OEM Group LLC., Gilbert, Arizona, 85233, USA*

³*Herbert Wertheim College of Engineering Research Service Centers, University of Florida, Gainesville, Florida 32611, USA*

Abstract

A fabrication process is developed for growth of c-axis textured aluminum nitride (AlN) film on the sidewall of single crystal silicon (Si) micro-fins to realize fin bulk acoustic wave resonators (FinBAR). FinBARs enable ultra-dense integration of high quality-factor (Q) resonators and low-loss filters on a small chip footprint and provide extreme lithographical frequency scalability over ultra- and super-high-frequency regimes. Si micro-fins with large aspect ratio are patterned and their sidewall surfaces are atomically smoothed. The reactive magnetron sputtering AlN deposition is engineered to optimize the hexagonal crystallinity of the sidewall AlN film with c-axis perpendicular to the sidewall of Si micro-fin. The effect of bottom metal electrode and surface roughness on the texture and crystallinity of the sidewall AlN film is explored. The atomic-layer-deposited platinum film with (111) crystallinity is identified as a suitable bottom electrode for deposition of c-axis textured AlN on the sidewall with c-axis orientation of $88.5^\circ \pm 1.5^\circ$ and arc-angle of $\sim 12^\circ$ around (002) diffraction spot over film thickness. 4.2 GHz FinBAR prototype is implemented showing a Q of 1,574 and effective electromechanical coupling (k_{eff}^2) of 2.75%, when operating in 3rd width-extensional resonance mode. The lower measured Q and k_{eff}^2 compared to simulations highlights the effect of granular texture of sidewall AlN film on limiting the performance of FinBARs. The developed c-axis textured sidewall AlN film technology paves the way for realization and monolithic integration of multi-frequency and multi-band FinBAR spectral processors for the emerging carrier aggregated wireless communication systems.

I. Introduction

Dense integration of multi-frequency and multi-band acoustic spectral processor is essential for realization of the emerging ultra-wideband mobile communication systems that operate based on carrier aggregation. These systems require a large set of resonators with frequencies over ultra- and super-high-frequency regimes to enable spread-spectrum data communication with minimum latency^{1,2}. Current radio frequency bulk acoustic wave (BAW) resonator technologies rely on planar architectures, such as film bulk acoustic resonators (FBAR) or solidly mounted resonators (SMR), with large surfaces to accommodate the required electromechanical transduction area for low-loss operation. The frequency of planar BAW resonators is tied to the thickness of the piezoelectric transducer film that is constant across the substrate. This substantial limitation prevents single-chip integration of multi-frequency and multi-band spectral processors needed for carrier aggregation. Furthermore, planar BAW resonators occupy large chip area since their loss is inversely proportional to the electroded surface dimensions of the piezoelectric film. This becomes more pronounced in carrier aggregation schemes that require several spectral processors at

^{a)} Electronic mail: rtabrizian@ufl.edu.

various frequencies and impose excessive integration costs and challenges^{2,3}. An alternative architecture that radically miniaturizes the planar footprint relies on integration of aluminum nitride (AlN) piezoelectric film transducers on the sidewall of silicon fins to realize high-performance fin bulk acoustic resonators (FinBAR)⁴. FinBARs enable ultra-dense integration of high Q resonators and filters in a small chip footprint. Furthermore, operating in width-extensional bulk acoustic modes, their frequency can be lithographically tailored over wide spectrums in ultra- and super-high-frequency regimes. FinBARs are ideally poised to provide a superior $k_{eff}^2 \cdot Q$, compared to planar BAW and contour mode resonators⁵, due to the low acoustic dissipation in Si and the large d_{33} of AlN sidewall transducer film. In practice, however, the performance of FinBAR is limited by the texture and crystalline orientation of sidewall AlN film. In this paper, process conditions for growth of densely textured AlN films with perpendicular c -axis on the sidewall of Si micro-fins are investigated, and the resulting films are characterized using scanning and transmission electron microscopy (SEM and TEM), and FinBAR prototypes.

II. Experimental

To facilitate investigation of the process for growth of c -axis textured sidewall AlN films, micro-fin structures are created on (110) Si substrate. Si micro-fins with various aspect ratio and distribution density are fabricated using Bosch DRIE process. Due to the essence of this process, which consists of a finite number of isotropic etch and passivation cycles, the sidewall surface of micro-fins suffers from large roughness and scalloping. Figure 1(a) shows the cross-sectional SEM of the Si micro-

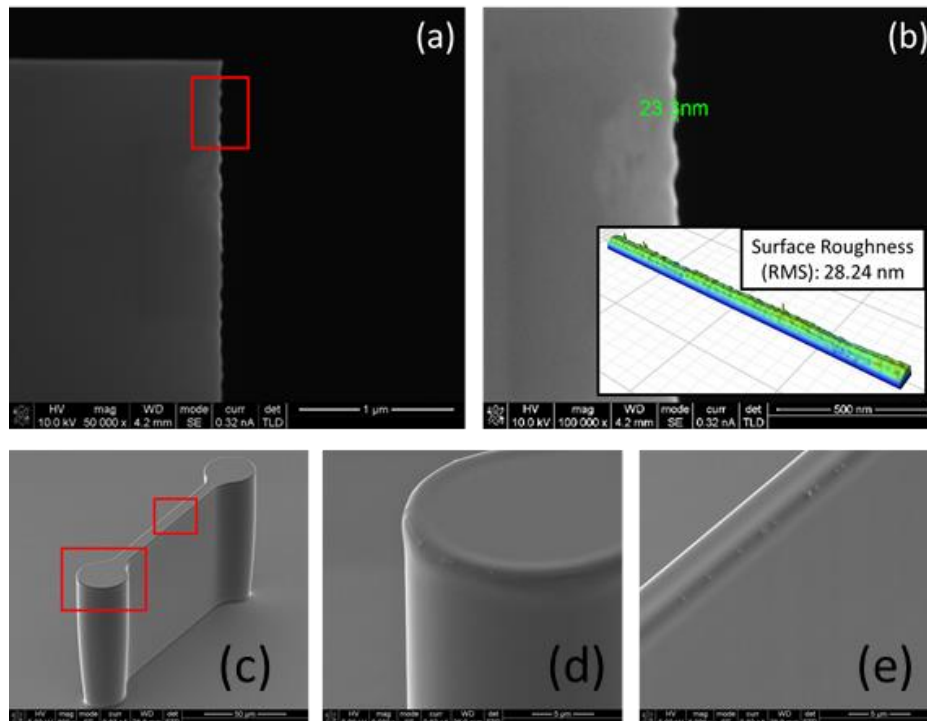


FIGURE 1. The cross-sectional SEM of the fin highlighting (a) the rough sidewall after Si DRIE and (b) the sidewall profile and surface roughness measured by Bruker Optical Profilometer . (c-e) The SEM of Si micro-fins after H₂ annealing illustrating the smooth sidewall surfaces at different regions.

fins after DRIE, highlighting a scallop depth of 23 nm. Figure 1(b) shows the sidewall topography measured using a Bruker Optical Profilometer tool, highlighting a surface roughness of ~28 nm in root-mean-square (rms). While achieving a high quality AlN films requires sub-1 nm surface roughness^{6,7}, hydrogen (H₂) annealing at 1100°C is used to smoothen sidewalls⁸. Figure 1(c-e) shows the micro-fins after H₂ annealing process. Four wafers with smoothened micro-fins are prepared. For the first and the second wafers (wafer 1 and wafer 2), the process is followed immediately with AC reactive magnetron sputtering of AlN on Si substrate with micro-fins. The third and the fourth wafers (wafer 3 and wafer 4) are used to study the effect of bottom electrodes on the texture of sidewall AlN films. On wafer 3, a 30 nm crystalline platinum (Pt) layer is atomically deposited in Cambridge Nano Fiji 200 Atomic Layer Deposition (ALD) tool at 150°C. On wafer 4, sputtered molybdenum (Mo) is deposited, on a 20 nm AlN seed layer, to serve as the bottom electrode. Endeavor PVD cluster tool is employed for the deposition of AlN and Mo thin films by AC and DC powered S-gun magnetrons, respectively. Two recipes are used for sputtering AlN on micro-fins in wafers 1 and 2. In both recipes, prior to AlN deposition, wafers are treated in RF plasma discharge at power of 70W ensuring effective argon (Ar) ion bombardment to atomically smoothen the fin surfaces^{9,10}. This is followed by AlN reactive sputtering at a base pressure of less than 2×10^{-7} mbar with a power of 5.5kW. In the first recipe (recipe 1), the Ar and nitrogen (N₂) gas flows of 5 and 17 SCCM are used respectively. In the second recipe (recipe 2), the Ar and N₂ gas flows are significantly reduced to 3 and 15 SCCM, respectively. The recipe 1 is used for the wafer 1 and the recipe 2 is used for the wafer 2, and also wafers 3 and 4, after deposition of bottom electrode layer. The processing is continued on wafer 3, towards fabrication of operational FinBARs, by sputtering of 150 nm Mo layer with a DC power of 3kW. This is followed by patterning the top Mo electrode on the sidewall of the micro-fins, and finally creation of access windows to the bottom Pt electrode through etching of AlN using tetramethylammonium hydroxide (TMAH) solution at 50°C. The electrical admittances are calculated from the S₁₁ scattering parameters. To de-embed the effect of electrical feed-through on probing pads and parasitic resistance of the routing lines, planar calibration structures are used.

III. Results and Discussion

A challenge with characterization of sidewall AlN films is the incapability of X-ray diffraction (XRD) for morphological study. This limitation is due to the small sidewall surface of micro-fins compared to the spot size of the optical ray, which prevents from local characterization of crystal content and orientation. In the absence of XRD results for sidewall AlN films, selected-area diffraction patterns, extracted from TEM images, are used¹¹. A detailed set of bright-field cross-sectional transmission electron microscopy (BF-XTEM) images, taken across the sidewall film thickness, are used to identify the relative quality of the films over process variations, and also when compared with the films deposited on the planar surfaces in the same deposition run.

A. Optimization of Sidewall AlN Deposition Process

Figure 2 (a) compares the SEM images of the planar and sidewall AlN films for wafers 1 and 2. The two processes used for deposition of AlN on these wafers differentiated in the Ar and N₂ pressures. In both wafers, the thickness of sidewall films were nearly a third of the planar films. The slower deposition rate on the sidewall can be attributed to the geometric factor reducing flux of sputter species to the sidewall compared to a plane wafer surface^{12,13}. Figure 2 (b) compares the TEM image of the planar and sidewall AlN films for wafers 1 and 2. From SEM and TEM images, it is evident that sputtering on sidewall results in tilted grains. Such titled growth can be attributed to the reduced mobility of ad-atoms on the sidewall and the increasing roughness of the film over the thickness^{14,15}. These in turn correspond to the non-perpendicular direction of the deposition flux and slowed nucleation of the sidewall film that resulted in growth of thick amorphous aluminum silicide (Al_xSi_{1-x}) layer at the interface with Si surface. This can be clearly observed comparing the TEM images of the planar and sidewall films in both processes. While the Al_xSi_{1-x} layer thickness is only 2 nm in planar films, its thickness increases to ~20 nm on the sidewall. The thicker amorphous Al_xSi_{1-x} layer results in excessive roughness of the sidewall surface, which in turn promotes tilted growth in individual grains¹⁶.

Comparing the SEM and TEM images for two processes it is evident that reduction in sputtering gas pressure significantly reduces the tilt angle of the grains. While the tilt angle of sidewall AlN grains in the process 1 is ~41°, it is ~53° for the process 2 with lowered deposition pressure. Figure 3 (a,b) compares the Fast Fourier transform (FFT) of the high-resolution XTEM, over selective locations across the thickness, for the sidewall films in wafers 1 and 2. The c-axis orientation, with respect to the surface is extracted for 20 locations uniformly distributed over the sidewall film thickness (Figure 3(c)). The c-axis orientation deviates from sidewall surface normal with thickness increase. C-axis orientations of 80.15°±8.15° for wafer 1 and 87.5°±1.5° for wafer 2 are extracted across the sidewall film thickness. This result highlights the significant improvement in normal

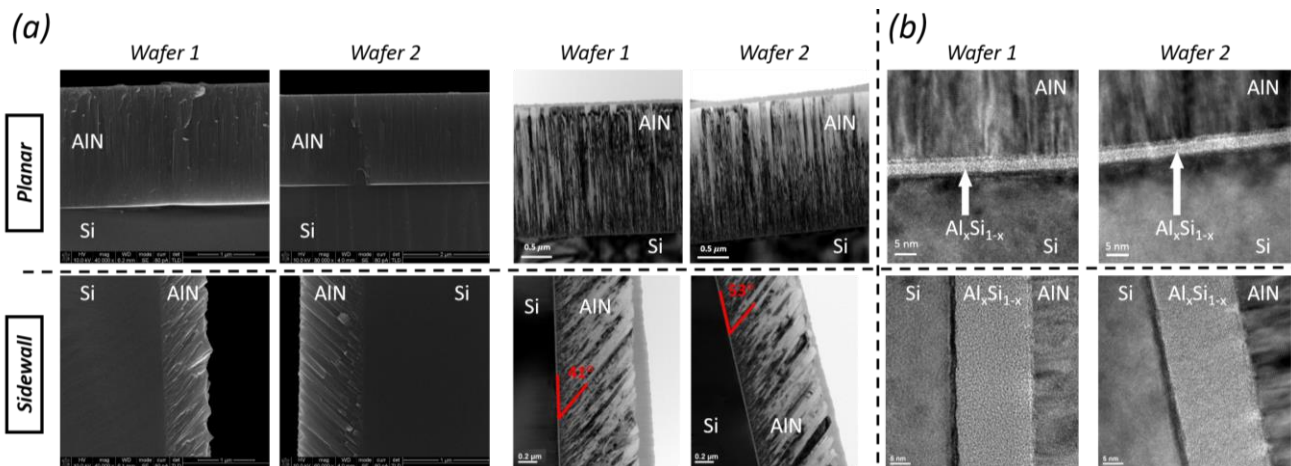


FIGURE 2. The (a) SEM and (b) TEM image of planar and sidewall AlN films deposited on wafers 1 and 2. (c) The TEM image at the interface with planar and sidewall Si surface highlighting the amorphous Al_xSi_{1-x} layer.

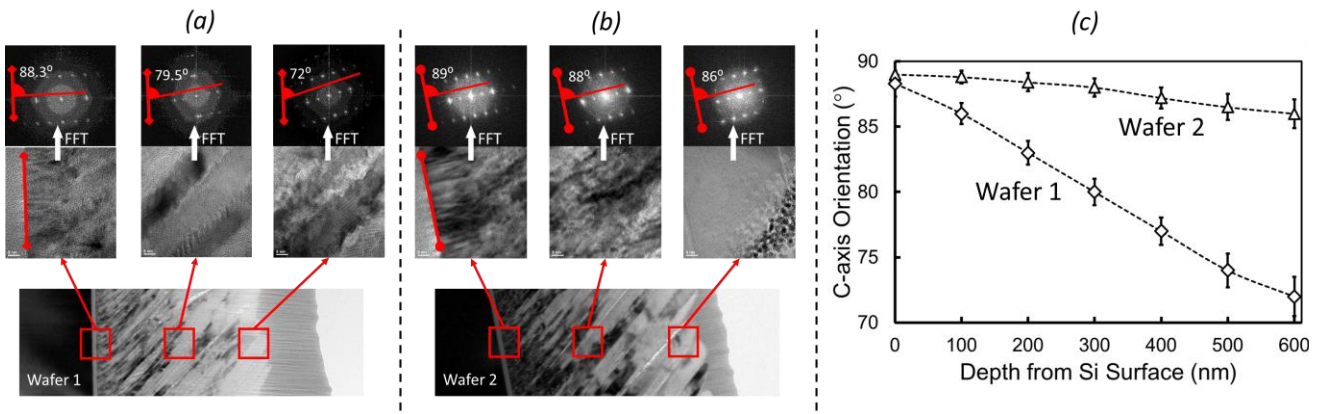


FIGURE 3. The FFT of high-resolution XTEM extracted from TEM images for sidewall AlN films in (a) wafer 1 and (b) wafer 2. (c) Comparison of C-axis orientation over the sidewall AlN thickness for wafers 1 and 2. The data is collected over 20 different cross-lines.

orientation and cross-thickness consistency of sidewall AlN c-axis with the reduction of sputtering pressure. Furthermore, the lower sputtering pressure results in improved crystallinity of the sidewall film. Figure 4 compares the arc-angle around (002) spot extracted from the diffraction patterns of sidewall films at 300 nm depth, for wafers 1 and 2. Arc-angles of $\sim 21^\circ + 10^\circ$ and $\sim 11^\circ + 6.3^\circ$ are measured for the wafers 1 and 2, respectively, which highlights the improvement in sidewall film crystallinity with lowered sputtering pressure.

Finally, figure 5 shows the SEM and compares the surface roughness of the sidewall AlN films for wafers 1 and 2. The sidewall films have significantly higher roughness compared to planar counterparts in both wafers. This is due to the granular growth of sidewall films. Furthermore, the surface roughness is significantly decreased by reducing the sputtering pressure in process 2. While a surface roughness of 158 nm (rms) is measured on the sidewall film in wafer 1, reducing the sputtering pressure results in a surface roughness of 29 nm (rms) in wafer 2.

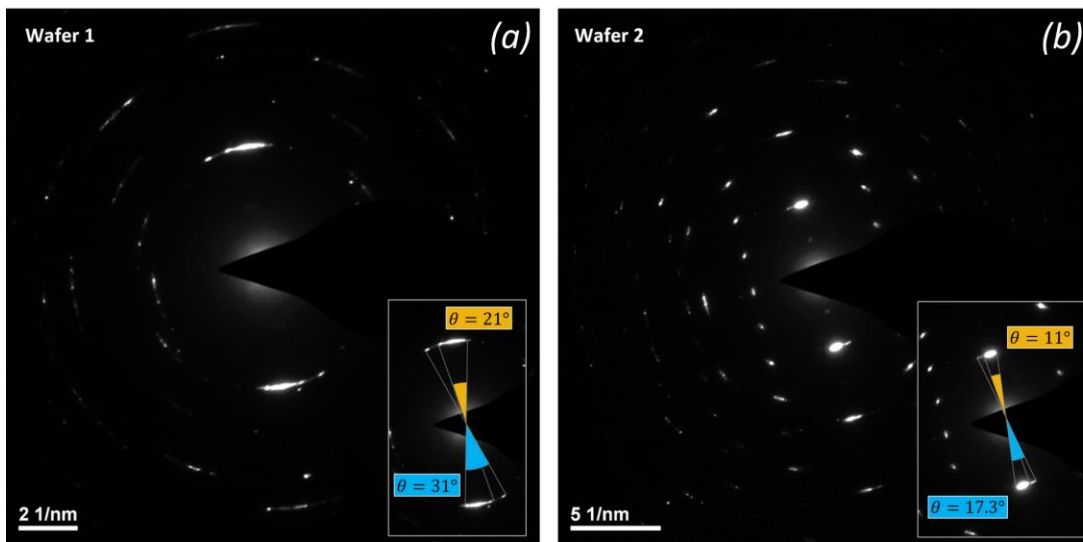


FIGURE 4. The FFT of high-resolution diffraction patterns at the 300 nm depth of sidewall AlN films in (a) wafer 1 and (b) wafer 2. The inset images show the arc-angle around (002) spot.

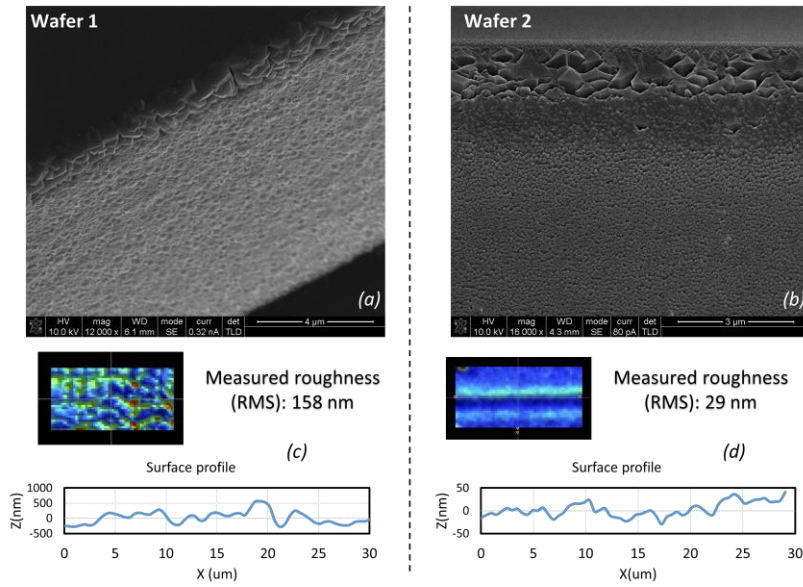


FIGURE 5. The SEM images of the sidewall AlN films deposited on (a) wafer 1 and (b) wafer 2. The measured surface roughness of the film for (c) wafer 1 and (d) wafer 2.

B. Effect of Bottom Electrode

Following the optimization of the sputtering process on Si micro-fins, wafers 3 and 4 are used to explore the effect of different bottom electrodes on the texture and crystallinity of the sidewall films. Considering the higher quality of sidewall films sputtered at lower pressure, the process 2 is used for AlN deposition on wafers 3 and 4. It is well-known that addition of bottom electrode tremendously affects the quality of sputtered piezoelectric film⁸⁻¹⁰. The choice of bottom electrode material and deposition methodology is identified to ensure crystalline texture of the metallic film. In wafer 3, a 30 nm ALD Pt that is deposited on (110) Si shows a dominant (111) texture (0.1° FWHM on the top surface). In wafer 4, a seed AlN layer of ~20 nm is sputtered on the sidewall, using process 2, to promote (110)-crystalline growth of the bottom Mo layer. Figure 6 compares the TEM image of the sidewall bottom electrodes for wafers 3 and 4. While the ALD Pt has created a sharp interface with Si sidewall surface, the amorphous Al_xSi_{1-x} layer with a thickness of 20 nm is evident in wafer 4 and results in granular growth of bottom Mo with large roughness. Figure 7 compares the TEM image of the subsequent AlN layer deposited on the bottom electrodes in wafers 3 and 4. While wafer 3 with ALD Pt electrode shows a crystalline texture across the sidewall film

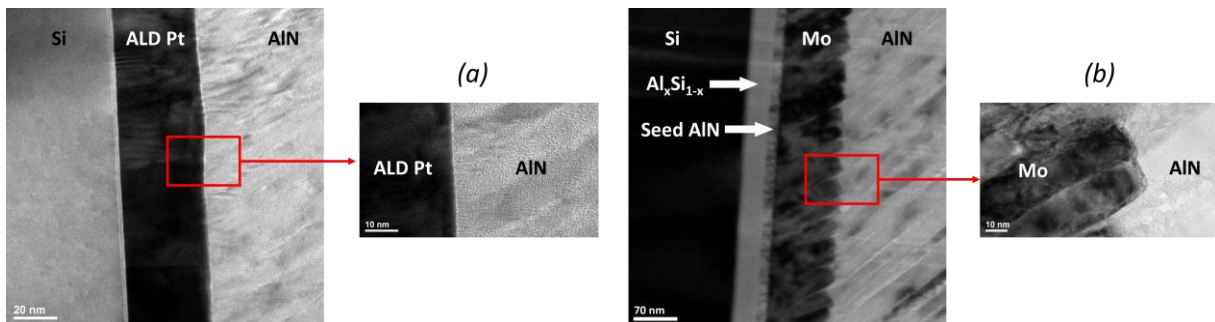


FIGURE 6. The TEM images of the sidewall bottom electrode deposited on (a) wafer 1 and (b) wafer 2.

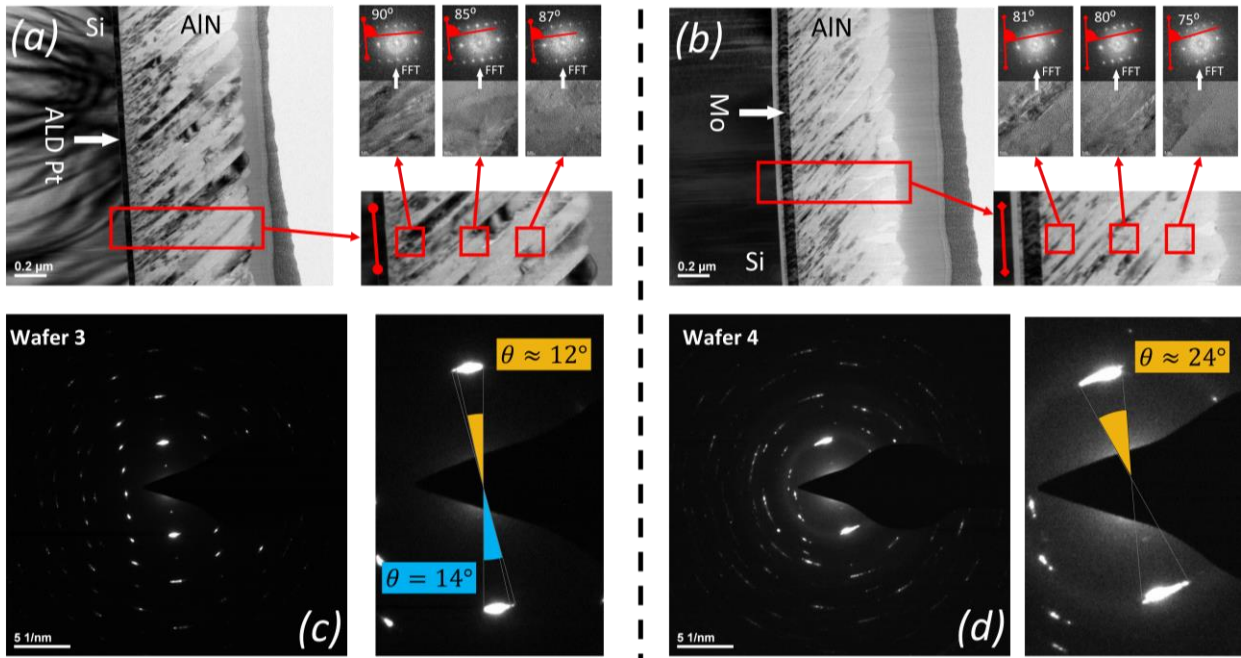


FIGURE 7. The TEM image and FFT of diffraction patterns for the sidewall AlN film deposited on the bottom electrodes for (a) wafer 1 and (b) wafer 2.

thickness, in wafer 4 the quality of sidewall AlN is substantially degraded as a result of bottom Mo roughness. A c-axis orientation of $88.5^{\circ} \pm 1.5^{\circ}$ and $78^{\circ} \pm 3^{\circ}$ is measured for wafers 3 and 4, respectively. Besides, the arc-angle of $12^{\circ} \pm 2^{\circ}$ and 24° are measured for wafers 3 and 4, respectively. While the quality of the sidewall film in wafer 4 is not suitable for implementation of FinBARs, the wafer 3 that utilize ALD Pt as the bottom electrode shows a comparable crystallinity to wafer 2 (no bottom electrode). Finally, figure 8 compares the surface roughness between wafers 2 and 3. While a similar c-axis orientation and crystallinity is observed in wafers 2 and 3, the addition of Pt bottom electrode has considerably reduced the surface roughness

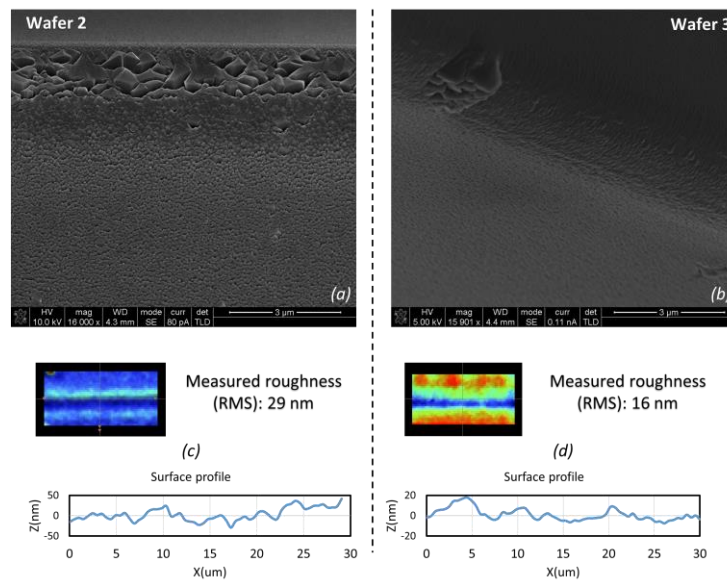


FIGURE 8. The SEM images of the sidewall AlN films deposited on (a) wafer 2 and (b) wafer 3. The measured surface roughness of the film for (c) wafer 2 and (d) wafer 3.

from 29 nm rms (wafer 2) to 16 nm rms (wafer 3). This improvement can be attributed to the effect of Pt layer as the diffusion barrier that prevents from formation of the rough and amorphous $\text{Al}_x\text{Si}_{1-x}$ layer at Si interface.

IV. FinBAR characterization

FinBARs are fabricated on wafer 3 through deposition and patterning of sidewall Mo electrodes and opening access to bottom Pt electrode. Figure 9(a) shows the SEM image of a FinBAR with 2.2 μm -wide fin, 30 nm ALD Pt as bottom electrode, 720 nm sidewall AlN, and 50 nm Mo as the top electrode on the sidewall. Figure 9(b) illustrates the measured admittance of the FinBAR, after de-embedding excessive pad capacitance and routing resistances, and compares it with COMSOL simulations. The FinBAR is operating in 3rd width-extensional mode at 4.23 GHz showing a Q of 1,574 and k_{eff}^2 of 2.75%, which are both smaller compared to simulations that show a Q of 2,600 (considering intrinsic acoustic dissipation in different materials and also the energy leakage into the substrate) and k_{eff}^2 of 3.78%. The lower k_{eff}^2 and Q of the measured FinBAR can be attributed to the lower quality of sidewall AlN compared to the ideal case. Specifically, the granular texture of the sidewall AlN film results in excessive intragranular boundaries that disperse the bulk acoustic vibration and induce excessive loss and charge cancellation that reduce Q and k_{eff}^2 .

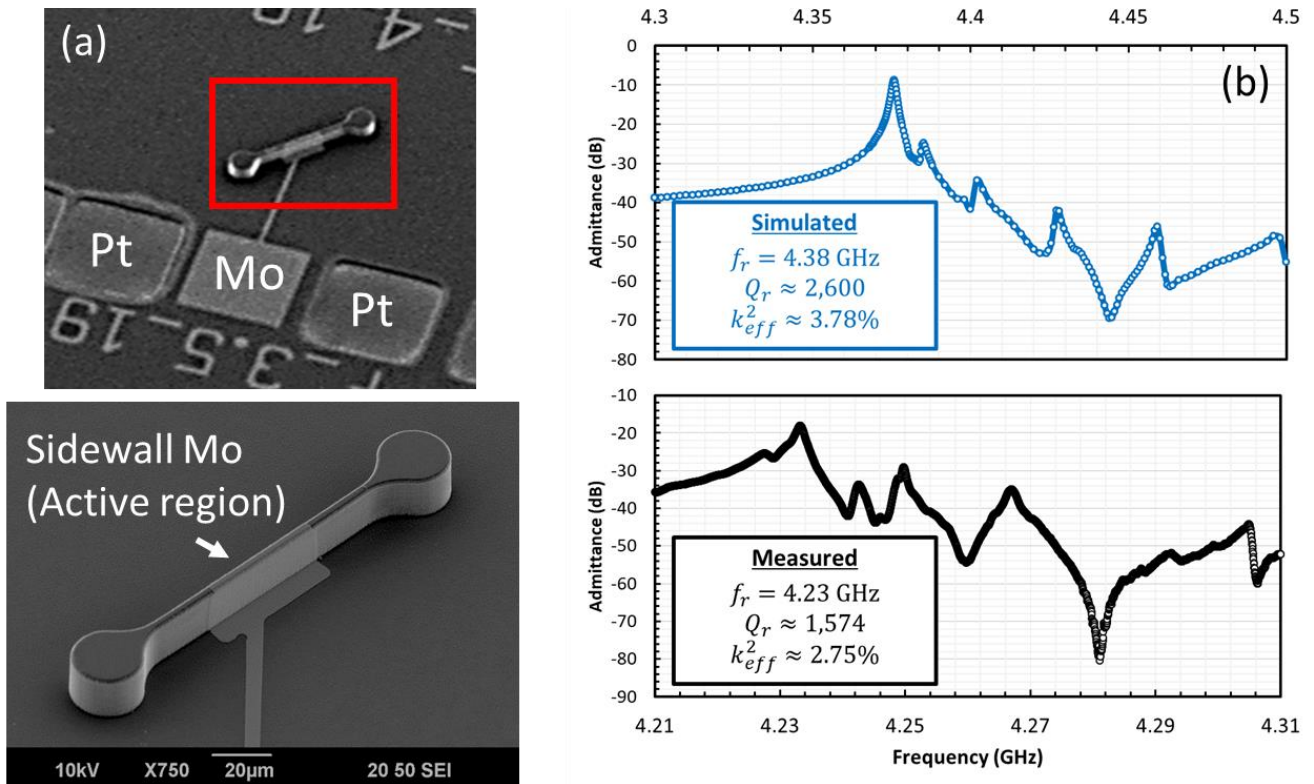


FIGURE 9. (a) The SEM image of a FinBAR implemented on wafer 3. (b) Simulated and measured admittance of the FinBAR.

V. Summary and Conclusion

This paper presents the process optimization of c-axis textured sidewall AlN films. These films enable realization of FinBAR technology that is poised to realize single-chip multi-band spectral processors. Highly c-axis oriented sidewall AlN films are achieved through low-pressure reactive magnetron sputtering. (111)-textured ALD Pt is used as the bottom electrode on the sidewall to suppress formation of amorphous $\text{Al}_x\text{Si}_{1-x}$ layer and facilitate crystalline growth of AlN with perpendicular c-axis orientation. This in turn reduced the surface roughness of the sidewall AlN film to ~ 16 nm. A 4.2 GHz FinBARs fabricated based on the optimized sidewall AlN process shows a Q of 1,574 and k_{eff}^2 of 2.75% that are smaller compared to simulations. The lower Q and k_{eff}^2 can be attributed to excessive intragranular surfaces in sidewall AlN that disperse the bulk acoustic vibration. Further work is needed to improve the quality of sidewall films to achieve FinBAR performances required for adoption in RF front-end applications.

Acknowledgements

This work was supported in part by the NSF grants ECCS 1752206.

References

1. Ruby, R., 2015. A snapshot in time: The future in filters for cell phones. *IEEE Microwave Magazine*, 16(7), pp.46-59.
2. Aigner, R., Fattinger, G., Schaefer, M., Karnati, K., Rothemund, R. and Dumont, F., 2018, December. BAW filters for 5G bands. In *2018 IEEE International Electron Devices Meeting (IEDM)* (pp. 14-5). IEEE.
3. Fattinger, G.G., Volatier, A., Al-Joumayly, M., Yusuf, Y., Aigner, R., Khlat, N. and Granger-Jones, M., 2016, May. Carrier aggregation and its challenges-or: The golden age for acoustic filters. In *2016 IEEE MTT-S International Microwave Symposium (IMS)* (pp. 1-4). IEEE.
4. Ramezani, M., Ghatge, M. and Tabrizian, R., 2017, December. High-Q silicon fin bulk acoustic resonators for signal processing beyond the UHF. In *2017 IEEE International Electron Devices Meeting (IEDM)* (pp. 40-1). IEEE.
5. Piazza, G., Stephanou, P.J. and Pisano, A.P., 2006. Piezoelectric aluminum nitride vibrating contour-mode MEMS resonators. *Journal of Microelectromechanical systems*, 15(6), pp.1406-1418.
6. Artieda, A., Barbieri, M., Sandu, C.S. and Mural, P., 2009. Effect of substrate roughness on c-oriented AlN thin films. *Journal of applied physics*, 105(2), p.024504.
7. Felmetzger, V.V., Laptev, P.N. and Graham, R.J., 2011. Deposition of ultrathin AlN films for high frequency electroacoustic devices. *Journal of Vacuum Science & Technology A: Vacuum, Surfaces, and Films*, 29(2), p.021014.

8. Lee, M.C. and Wu, M.C., 2006. Thermal annealing in hydrogen for 3-D profile transformation on silicon-on-insulator and sidewall roughness reduction. *Journal of Microelectromechanical systems*, 15(2), pp.338-343.
9. Labanda, J.G.C., Barnett, S.A. and Hultman, L., 1998. Damage-free cleaning of Si (001) using glancing-angle ion bombardment. *Journal of Vacuum Science & Technology B: Microelectronics and Nanometer Structures Processing, Measurement, and Phenomena*, 16(4), pp.1885-1890.
10. Felmetzger, V.V., Mikhov, M.K. and Laptev, P.N., 2015. Effect of pre-deposition rf plasma etching on wafer surface morphology and crystal orientation of piezoelectric AlN thin films. *IEEE transactions on ultrasonics, ferroelectrics, and frequency control*, 62(2), pp.387-391.
11. Williams, D.B. and Carter, C.B., 1996. The transmission electron microscope. In *Transmission electron microscopy* (pp. 3-17). Springer, Boston, MA.
12. Blech, I.A. and Vander Plas, H.A., 1983. Step coverage simulation and measurement in a dc planar magnetron sputtering system. *Journal of Applied Physics*, 54(6), pp.3489-3496.
13. Martin, F., Jan, M.E., Rey-Mermet, S., Belgacem, B., Su, D., Cantoni, M. and Muralt, P., 2006. Shear mode coupling and tilted grain growth of AlN thin films in BAW resonators. *IEEE transactions on ultrasonics, ferroelectrics, and frequency control*, 53(7), pp.1339-1343.
14. Müller, K.H., 1987. Role of incident kinetic energy of adatoms in thin film growth. *Surface science*, 184(1-2), pp.L375-L382.
15. Marinov, M., 1977. Effect of ion bombardment on the initial stages of thin film growth. *Thin Solid Films*, 46(3), pp.267-274.
16. DeMiguel-Ramos, M., Clement, M., Olivares, J., Capilla, J., Sangrador, J. and Iborra, E., 2013, July. Induced surface roughness to promote the growth of tilted-AlN films for shear mode resonators. In *2013 Joint European Frequency and Time Forum & International Frequency Control Symposium (EFTF/IFC)* (pp. 274-277). IEEE.
17. Lee, J.B., Jung, J.P., Lee, M.H. and Park, J.S., 2004. Effects of bottom electrodes on the orientation of AlN films and the frequency responses of resonators in AlN-based FBARs. *Thin Solid Films*, 447, pp.610-614.
18. Iriarte, G.F., Bjurstrom, J., Westlinder, J., Engelmark, F. and Katardjiev, I.V., 2005. Synthesis of c-axis-oriented AlN thin films on high-conducting layers: Al, Mo, Ti, TiN, and Ni. *IEEE transactions on ultrasonics, ferroelectrics, and frequency control*, 52(7), pp.1170-1174.
19. Xiong, J., Gu, H.S., Hu, K. and Hu, M.Z., 2010. Influence of substrate metals on the crystal growth of AlN films. *International Journal of Minerals, Metallurgy, and Materials*, 17(1), pp.98-103.